NeuroImage 226 (2021) 117581

Contents lists available at ScienceDirect

NeuroImage

journal homepage: www.elsevier.com/locate/neuroimage

Development of the default-mode network during childhood and adolescence: A longitudinal resting-state fMRI study

Fengmei Fan[a,b,c,d], Xuhong Liao[e,*], Tianyuan Lei[a,b,c], Tengda Zhao[a,b,c], Mingrui Xia[a,b,c], Weiwei Men[f,g], Yanpei Wang[a], Mingming Hu[a], Jie Liu[a], Shaozheng Qin[a,b,c], Shuping Tan[d], Jia-Hong Gao[f,g,h], Qi Dong[a], Sha Tao[a,*], Yong He[a,b,c,i,*]

[a] State Key Laboratory of Cognitive Neuroscience and Learning, Beijing Normal University, Beijing 100875, China
[b] Beijing Key Laboratory of Brain Imaging and Connectomics, Beijing Normal University, Beijing 100875, China
[c] IDG/McGovern Institute for Brain Research, Beijing Normal University, Beijing 100875, China
[d] Beijing Huilongguan Hospital, Peking University Huilongguan Clinical Medical School, Beijing 100096, China
[e] School of Systems Science, Beijing Normal University, Beijing 100875, China
[f] Center for MRI Research, Academy for Advanced Interdisciplinary Studies, Peking University, Beijing 100871, China
[g] Beijing City Key Laboratory for Medical Physics and Engineering, Institute of Heavy Ion Physics, School of Physics, Peking University, Beijing 100871, China
[h] IDG/McGovern Institute for Brain Research, Peking University, Beijing 100871, China
[i] Chinese Institute for Brain Research, Beijing 102206, China

ARTICLE INFO

Keywords:
Default-mode network
Children
Connectome
Development
Resting-state fMRI

ABSTRACT

The default-mode network (DMN) is a set of functionally connected regions that play crucial roles in internal cognitive processing. Previous resting-state fMRI studies have demonstrated that the intrinsic functional organization of the DMN undergoes remarkable reconfigurations during childhood and adolescence. However, these studies have mainly focused on cross-sectional designs with small sample sizes, limiting the consistency and interpretations of the findings. Here, we used a large sample of longitudinal resting-state fMRI data comprising 305 typically developing children (6–12 years of age at baseline, 491 scans in total) and graph theoretical approaches to delineate the developmental trajectories of the functional architecture of the DMN. For each child, the DMN was constructed according to a prior parcellation with 32 brain nodes. We showed that the overall connectivity increased in strength from childhood to adolescence and became spatially similar to that in the young adult group ($N = 61$, 18–28 years of age). These increases were primarily located in the midline structures. Global and local network efficiency in the DMN also increased with age, indicating an enhanced capability in parallel information communication within the brain system. Based on the divergent developmental rates of nodal centrality, we identified three subclusters within the DMN, with the fastest rates in the cluster mainly comprising the anterior medial prefrontal cortex and posterior cingulate cortex. Together, our findings highlight the developmental patterns of the functional architecture in the DMN from childhood to adolescence, which has implications for the understanding of network mechanisms underlying the cognitive development of individuals.

1. Introduction

The default-mode network (DMN) is a set of brain regions that consistently deactivate in external attention-demanding tasks (e.g., selective attention to external stimuli), including the posterior cingulate cortex (PCC)/precuneus, medial prefrontal cortex (mPFC), inferior parietal lobule, lateral temporal cortex, and hippocampal regions (Buckner et al., 2008; Buckner and DiNicola, 2019; Gusnard et al., 2001; Raichle, 2015; Raichle et al., 2001; Shulman et al., 1997). These regions are activated during internal mental processes, such as recalling autobiographical and episodic memories (Andrews-Hanna et al., 2014; Buckner et al., 2008), envisioning the future (Gilbert and Wilson, 2007), and making social inferences (Spreng et al., 2009). Resting-state functional MRI (rsfMRI) studies in healthy adults have revealed that the DMN regions are tightly functionally connected into a network (Fox et al., 2005; Greicius et al., 2003). These regions usually show a large number of functional connections and serve as functional hubs for global integration across the whole brain (Buckner et al., 2009; Liang et al., 2013; Liao et al., 2013; van den Heuvel and Sporns, 2013). Moreover, DMN

* Corresponding authors at: School of Systems Science, Beijing Normal University, Beijing 100875, China (Xuhong Liao); State Key Laboratory of Cognitive Neuroscience and Learning, Beijing Normal University, Beijing 100875, China (Sha Tao and Yong He).
E-mail addresses: liaoxuhong@bnu.edu.cn (X. Liao), taosha@bnu.edu.cn (S. Tao), yong.he@bnu.edu.cn (Y. He).

https://doi.org/10.1016/j.neuroimage.2020.117581
Received 1 August 2020; Received in revised form 4 November 2020; Accepted 12 November 2020
Available online 19 November 2020

connectivity strength is positively correlated with individual cognitive performances (e.g., working memory, autobiographical memory, attention, and language) (Hampson et al., 2006; Liu et al., 2017; Mevel et al., 2013; Persson et al., 2014; Prakash et al., 2012; Sambataro et al., 2010; Yang et al., 2013). Intriguingly, rather than being a single monolithic network as originally envisaged, the DMN consists of at least two subnetworks with specialized roles, including the separation of the ventral medial posterior cortex and medial temporal lobe (MTL) from other regions (Andrews-Hanna et al., 2010; Braga and Buckner, 2017; Braga et al., 2019; Buckner and DiNicola, 2019); this provides insights into the understanding of DMN subsystems that underlie different cognitive processes.

During childhood and adolescence, children rapidly develop their cognitive, emotional, and social capabilities (Bhana, 2010). They make important strides in internal mentation, including self-awareness (Rochat, 2011), autobiographical memory (Given-Wilson et al., 2018), moral judgment (Cushman et al., 2013), and theory of mind (Devine and Hughes, 2013; Dumontheil et al., 2010; O'Connor and Evans, 2019). Moreover, early adolescents experience "social reorientation", associated with increasing sensitivity to social cues and peer relationships and enhanced social learning ability in external cultures (Nelson et al., 2005). Improvements in these cognitive and social capabilities parallel the developmental refinements of the structural and functional organization within the brain (Blakemore et al., 2010; Casey et al., 2000; Sato et al., 2008). During this period, the brain's functional networks reconfigure from an anatomical-dominant structure to a distributed architecture (Fair et al., 2009), and functional hubs show strengthening connectivity strength (Hwang et al., 2013), suggesting increased functional integration during development. Considering that the DMN is closely related to internal mentation activity and social domain functions (Blakemore, 2008; Buckner and DiNicola, 2019; Raichle, 2015; Spreng et al., 2009), exploring the development of the functional organization of the DMN during childhood and adolescence will shed light on the neural mechanisms supporting individual cognitive development.

Several studies have investigated how the functional connectivity within the DMN develops in different age groups (de Bie et al., 2012; Fair et al., 2008; Rebello et al., 2018; Sato et al., 2014; Sherman et al., 2014; Xiao et al., 2016). The connectivity strength within the DMN is greater in older children than in younger children during childhood and adolescence (de Bie et al., 2012; Fair et al., 2008; Rebello et al., 2018; Sato et al., 2014; Sherman et al., 2014; Xiao et al., 2016) and is greater in adults than in children (Fair et al., 2008). Using a prior parcellation comprising three DMN subsystems, a recent study revealed subsystem inhomogeneity in development, wherein the MTL subsystem showed stronger functional connectivity strength in 5-year-old children than in 3-year-old children, but the other two subsystems showed no significant changes (Xiao et al., 2016). These studies provide crucial evidence for the enhanced functional integration and subsystem development within the DMN with increasing age. However, it should be noted that most of these studies employed a cross-sectional design, a small sample size (< 100), or narrow age ranges and that the interpretations of the findings should be treated with caution. To date, only one study has employed a longitudinal task-related fMRI dataset comprising 45 children (10–13 years old) and focused on the age-related changes in the functional connectivity of one region (i.e., the PCC) within the DMN (Sherman et al., 2014). A longitudinal study with a larger sample size is necessary to reduce the confounding effects of individual variability and improve statistical power (Bernal-Rusiel et al., 2013; Gaspar et al., 2015; Newman, 2010) and would provide a better description of the developmental trajectories of the DMN.

Here, we investigated the development of the functional architecture of the DMN from childhood to adolescence based on a large longitudinal rsfMRI sample comprising 305 children (6–12 years of age at baseline, 491 scans). We also included a sample of 61 young adults (18–28 years of age) for cross-sectional comparisons. A linear mixed model was used to characterize the age-related continuous change, which is applicable to the case of missing time points while simultaneously accounting for variability within and across participants (Kutluturk Karagoz et al., 2019; Laird and Ware, 1982). In the present study, we first constructed individual functional networks within the DMN comprising 32 nodes and then characterized the development of functional connectivity strength and topological properties using the graph theoretical approach. We investigated the regional heterogeneity in the developmental rate of degree centrality (i.e., total connectivity strength attached to a region), which was used to further identify subclusters within the DMN. We hypothesize that 1) the DMN becomes a more integrated and efficient network from childhood to adolescence, manifested in connectivity, global and regional properties; and 2) several subclusters of the DMN can be detected based on the divergent developmental rates in regional functional connectivity.

2. Materials and methods

2.1. Participants

We used a longitudinal rsfMRI dataset comprising 360 typically developing children aged 6.1–12.9 years (F/M = 163/197) from the Children School Functions and Brain Development project (CBD, Beijing Cohort). Some of these children underwent repeated MRI scans with an interval of approximately one year, leading to 643 MRI scans in total. All children were recruited from primary schools in Beijing and were cognitively normal, assessed by a well-validated Chinese standardized cognitive ability test (Dong and Lin, 2011). Exclusion criteria included significant physical illness or head injury and a history of neurological/psychiatric disorders. The children were prohibited from taking any drugs or caffeine on the day of the behavioral tests and MRI scans. After data quality control, 152 rsfMRI scans were excluded due to T1 artifacts (N = 40), field map errors (N = 6), excessive head motion (N = 94), and "bad" time points (N = 12) (for details, see data preprocessing). Finally, rsfMRI data of 305 children (6.2–12.4 years of age at baseline, F/M = 143/162, 491 scans in total, Fig. 1A) remained, wherein 3 scans were available for 47 children (F/M = 31/16), 2 scans were available for 92 children (F/M = 47/45) and 1 scan was available for 166 children (F/M = 65/101). To compare with adults, we additionally used an rsfMRI dataset comprising 62 healthy young adults (F/M = 37/25, 22.4 ± 2.4 years of age, range: 18.1–28.8 years), which was also collected by the project using the same procedure with the children. All adult participants were recruited through advertisements in Beijing. The exclusion criteria were the same as those for children. One adult was excluded due to field map error, and 61 adults (F/M = 37/24, 18.1–28.8 years of age) ultimately remained. All the children's parents/guardians and the adults provided written informed consent approved by the Ethics Committee of Beijing Normal University.

2.2. Image acquisition

Multimodal MRI data were collected in a Siemens Prisma 3T MRI scanner with a 64-channel head coil at Peking University, Beijing. During the scanning, foam pads were used to reduce the head motion of participants. The rsfMRI data were obtained with an echo-

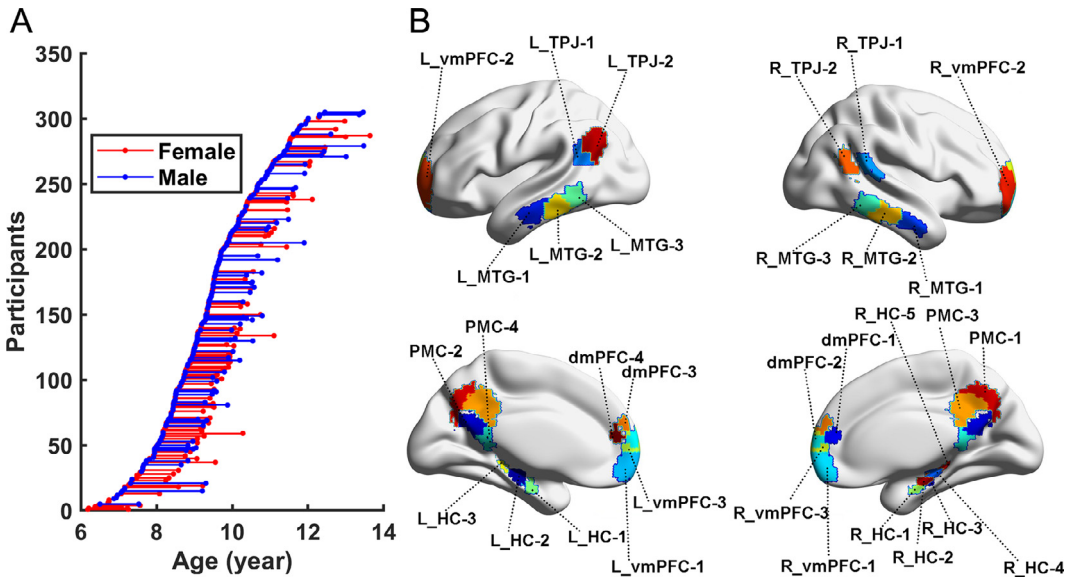

Fig. 1. Children's age at MRI scans and nodal definition of the default-mode network (DMN). (A) Children's age at MRI scans. Each dot denotes one child at each scan. Each line connects the repeated scans of the same individual. (B) Thirty-two DMN nodes obtained from a prior atlas provided in Kernbach et al. (2018) (https://identifiers.org/neurovault.collection:3434). In the prior parcellation, the spatial locations of the dmPFC and vmPFC partially overlapped. We removed the overlapping regions (i.e., ventral areas) from the dmPFC and obtained the modified nodes of the dmPFC. dmPFC, dorsal medial prefrontal cortex; vmPFC, ventromedial prefrontal cortex; PMC, posteromedial cingulate cortex; TPJ, temporoparietal junction; MTG, middle temporal gyrus; HC, hippocampus.

planar imaging sequence with the following parameters: repetition time (TR) = 2000 ms, echo time (TE) = 30 ms, flip angle (FA) = 90°, field of view (FOV) = 224 × 224 mm^2, matrix size = 64 × 64, axial slices = 33, thickness/gap = 3.5/0.7 mm, and volumes = 240 (8 min). During rsfMRI scanning, participants were instructed to relax and fixate on a bright cross-hair centered in the scanner screen. Prior to the rsfMRI scanning, the field map was acquired using a 2-dimensional dual gradient-echo sequence: TR = 400 ms, TE1 = 4.92 ms, TE2 = 7.38 ms, FA = 60°, FOV = 224 × 224 mm^2, matrix size = 64 × 64, axial slices = 33, and thickness/gap = 3.5/0.7 mm. T1-weighted structural images were acquired using a sagittal 3D-magnetization prepared rapid acquisition gradient echo (MPRAGE) sequence: TR = 2530 ms, TE = 2.98 ms, inversion time = 1100 ms, FA = 7°, FOV = 256 × 224 mm^2, matrix size = 256 × 224, slice thickness = 1 mm, and scan time = 5 min and 58 s.

2.3. Data preprocessing

For each child, functional data preprocessing was carried out using SPM12 (https://www.fil.ion.ucl.ac.uk/spm) and DPABI 3.0 (Yan et al., 2016). We first performed the removal of the first 10 volumes, slice timing correction, field map-based distortion correction and head motion correction. Ninety-four scans were excluded due to excessive head motion, with the maximal displacement above 3 mm, the maximal rotation above 3° or a mean framewise displacement (FD) across time (Power et al., 2012) greater than 0.5 mm. Twelve scans with more than 50 "bad" time points were further discarded, where the "bad" time points were defined as those with FD above 0.5 mm. Then, the individual functional images were coregistered with the T1 image and spatially normalized to a custom pediatric template. Specifically, the spatial normalization procedure was performed with four steps: i) the individual T1 images were segmented into gray matter, white matter, and cerebrospinal fluid tissue maps using the Chinese Pediatric Atlases (CHN-PD) (6–12 years) (Zhao et al., 2019) (https://www.nitrc.org/projects/chn-pd) as a reference; ii) the resulting spatially normalized tissue maps (i.e., gray matter, white matter, and cerebrospinal fluid maps) in CHN-PD space were separately averaged across all the scans to generate the custom tissue templates; iii) the individual T1 images were segmented again with the custom tissue templates as a reference; and iv) the individual functional images were spatially normalized to the custom space by applying transformation parameters estimated during the second T1 segmentation and were resampled to 3-mm isotropic voxels. The spatially normalized images were smoothed with a Gaussian kernel with a full-width half maximum value of 4 mm. Next, we performed linear detrend and nuisance signal regression, during which 24-parameter head motion parameters (Friston et al., 1996), "bad" time points with FD above 0.5 mm, white matter, cerebrospinal fluid, and global brain signals were included as covariates. Twelve scans were further excluded due to an excessive proportion of "bad" time points (i.e., more than 50 "bad" time points). Finally, temporal bandpass filtering (0.01–0.1 Hz) was performed.

For the adult group, rsfMRI data were preprocessed in the same way as those of the children except for the spatial normalization procedure, wherein the head motion corrected functional images were spatially normalized to Montreal Neurological Institute (MNI) space with a priori tissue maps provided in SPM12 as a reference.

2.4. Functional connectivity analysis of the DMN

Previous studies have pointed out that there are strong autocorrelations between the time series of a voxel and its neighbors, which may bias the estimation of voxelwise functional connectivity (Wig et al., 2011). To reduce the potential influence of autocorrelations and improve the reliability of the findings, we constructed the DMN at the regional level instead of using the voxelwise approach. To characterize the interregional functional connectivity within the DMN, we defined 32 nodes of interest according to a prior parcellation (Kernbach et al., 2018) (Fig. 1B), including 4 nodes in the dorsal medial prefrontal cortex (dmPFC), 6 nodes in the ventromedial prefrontal cortex (vmPFC), 4 nodes in the posteromedial cingulate cortex (PMC), 4 nodes in the bilateral temporoparietal junction (TPJ), 6 nodes in the bilateral middle temporal gyrus (MTG), and 8 nodes in the bilateral hippocampus (HC). Since there are partial overlaps between the dmPFC and vmPFC nodes in the prior parcellation, we removed the overlapping areas (i.e., ventral areas) from the dmPFC and obtained four new dmPFC nodes. Of note,

for the children, the prior parcellation in MNI space was transformed into the children's custom space by applying parameters determined by normalizing the prior T1 template in MNI space (provided in SPM12) to the children-specified T1 template.

Based on the above procedure, we examined the functional connectivity patterns among the 32 nodes in the DMN for each scan of each individual. Briefly, we extracted the mean time course for each node and estimated the individual DMN functional connectivity matrices (i.e., a 32×32 matrix) by calculating the pairwise Pearson's correlation coefficient between nodal time courses. Next, we estimated the mean connection strength within the DMN to characterize the overall connectivity strength. We also estimated the spatial similarity of functional connectivity patterns in the children with the representative pattern (i.e., the group-averaged pattern) of the adult group to quantify the maturation extent of the overall connectivity pattern. For each child, the spatial similarity with the adults' pattern was measured by Pearson's correlation coefficients across all the lower triangular elements between two connectivity matrices of interest. To characterize the changes in the functional connectivity patterns during development, we estimated the age effect on connectivity strength using a linear mixed model (for details, see "Statistical analysis"). For connectivities showing significant age effects, we also examined the potential influence of internode Euclidean distance on developmental changes.

2.5. Network topology analysis of the DMN

To characterize the topological properties of the DMN, we estimated several of its global and nodal network metrics. Prior to the network analysis, we generated individual weighted functional networks by applying a correlation threshold r_{th} of 0.2 to remove the spurious correlations. To assess the potential influence of the correlation threshold on the brain network topology, we also considered two other thresholds (i.e., 0.1 and 0.3) in the validation analysis.

i) *Global metrics.* We calculated the global efficiency (E_{glob}) and local efficiency (E_{loc}) (Latora and Marchiori, 2001; Onnela et al., 2005) of the DMN. E_{glob} represents the efficiency of the parallel information transfer among all possible pairs of nodes in the network. Given a network G, E_{glob} is defined as follows:

$$E_{glob}(G) = \frac{1}{N(N-1)} \sum_{i \in G} \sum_{j \neq i \in G} \frac{1}{L_{ij}}, \tag{1}$$

where L_{ij} is the shortest path length between node i and node j in network G, and N denotes the number of nodes in the DMN (i.e., $N = 32$). E_{loc} measures the communication efficiency among the nearest neighbors of a node when it is removed, which captures the fault tolerance of the network. Given a network G, E_{loc} is defined as follows:

$$E_{loc}(G) = \frac{1}{N} \sum_{i \in G} E_{glob}(G_i), \tag{2}$$

where G_i denotes the subgraph composed of the nearest neighbors of node i.

ii) *Nodal metrics.* We first quantified the topological importance of nodes using degree centrality, the most common metric of nodal centrality, to characterize the straightforward influence of nodes in the network (van den Heuvel and Sporns, 2013). In the weighted network, degree centrality is defined as follows:

$$DC_{nodal}(i) = \sum_{i \neq j \in G} W_{ij}, \tag{3}$$

where W_{ij} is the connectivity strength between nodes i and j. A node with high degree centrality means that this node interacts with many other nodes in the network. In addition, we computed the nodal efficiency (Achard and Bullmore, 2007) for each node to characterize the regional capability in parallel information communication. Given a node i, the nodal efficiency $E_{nodal}(i)$ is defined as follows:

$$E_{nodal}(i) = \frac{1}{N-1} \sum_{j \neq i \in G} \frac{1}{L_{ij}}, \tag{4}$$

where L_{ij} is the shortest path length between node i and node j in the network.

2.6. Statistical analysis

i) *Effects of age on network properties in children.* To quantify the effects of age on the measurements of interest (i.e., connectivity strength, connectivity pattern similarity, and network metrics), we used a linear mixed model (Laird and Ware, 1982), which can characterize the age-related continuous change and is applicable to instances of missing time points. Considering the potential linear or quadratic effects of age, we employed two types of statistical models, which separately included the linear and quadratic terms as the highest order terms. Sex and mean FD were included as covariates in the models. Specifically, the linear model is defined as follows:

$$\begin{aligned} Y_{ij} &= \beta_0 + b_i + (\beta_{age} + b_{age,i}) age_{ij} + \beta_{sex} Sex_i + \beta_{mFD} mFD_{ij} \\ &\quad + \varepsilon_{ij}, i = 1, 2, \ldots, N \end{aligned} \tag{5}$$

The quadratic model is defined as follows:

$$\begin{aligned} Y_{ij} &= \beta_0 + b_i + (\beta_{age1} + b_{age,i1}) age_{ij} + (\beta_{age2} + b_{age,i2})\, age_{ij}^2 + \beta_{sex} Sex_i \\ &\quad + \beta_{mFD} mFD_{ij} + \varepsilon_{ij}, i = 1, 2, \ldots, N \end{aligned} \tag{6}$$

In these two equations, Y_{ij} represents the measurement of subject i at the jth scan, β_{age} represents the fixed age effect, $b_{age,i}$ represents the random effect, and ε_{ij} represents the residual. To determine which model (i.e., the linear or quadratic model) better captures the age effects, we used the Akaike information criterion (AIC) value (Akaike, 1974) to select the best-fit model. The AIC index reflects a trade-off between the likelihood and simplicity (i.e., independent variables) of a model. In accordance with Akaike's theory, the model with the lower AIC value was chosen as the optimal model. To correct for multiple comparisons, we used a false discovery rate (FDR) procedure. A q value of 0.05 was determined for the age effect on connectivity strength, nodal degree, and nodal efficiency.

ii) *Sex effects.* To explore the sex difference in the DMN topology and the developmental changes, we utilized the following linear mixed model, which included sex and age-by-sex interaction terms as predictors:

$$\begin{aligned} Y_{ij} &= \beta_0 + b_i + (\beta_{age} + b_{age,i}) age_{ij} + \beta_{sex} sex_i + \beta_{age*sex}(age_{ij} * sex_i) \\ &\quad + \beta_{mFD} mFD_{ij} + \varepsilon_{ij}, i = 1, 2, ..., N \end{aligned} \tag{7}$$

Similar to the age effect analysis, the significant effects of sex and age-by-sex interaction were also assessed using the FDR procedure ($q < 0.05$) to correct for multiple comparisons.

iii) *Group comparisons of children vs. adults.* To examine how the measurements showing significant effects of age differed between the children and the adults, we further performed a two-sample t-test between the two groups. Since some children underwent repeated rsfMRI scans during the longitudinal design, only the measurements at baseline were included during the two-sample t-test analysis to exclude the potential correlation between samples.

2.7. Identifying DMN subclusters using developmental rates of nodal centrality

Previous studies have suggested regional heterogeneity of the DMN in development (Xiao et al., 2016), indicating the potential functional specialization in DMN development. To identify the DMN subclusters with similar developmental rates, we used a data-driven k-means clustering algorithm (Seber, 2009). The developmental rate (beta value) of

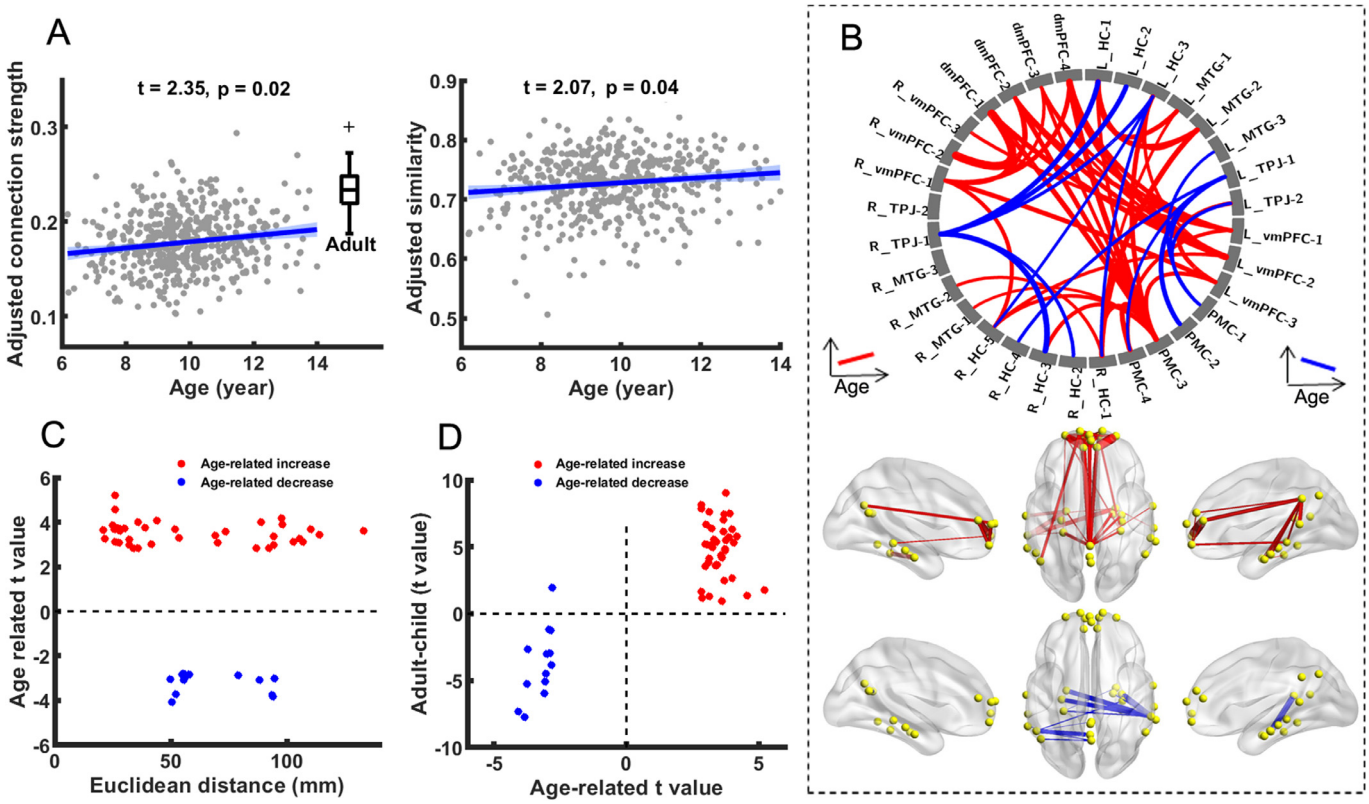

Fig. 2. Development of DMN functional connectivity in children from 6 to 14 years old. (A) Developmental trajectories of the mean connectivity strength (left panel) and the spatial similarity of the connectivity pattern with the adults (right panel). In both panels, the dots represent the adjusted values of each child after regressing out sex and head motion. The boxplot in the left panel illustrates the median (horizontal line), 25th and 75th percentiles (box) and nonoutlier range (whiskers) for the adjusted values in the adult group. Significantly higher connectivity strength was observed in the adults than in the children. (B) Spatial distributions of significantly changed functional connectivities. Red and blue colors represent significant age-related increases and decreases, respectively. Line thickness represents the significance level of the age effect in terms of [–log10(p)]. Multiple comparisons were corrected using the FDR method with a significance level of $q < 0.05$. (C) Scatter plot of the age effect versus interregional Euclidean distance. (D) Scatter plot of the age effect versus the group difference between the children and the adults.

each DMN nodal degree was set as the clustering feature, and the distance between any two regions was defined as the Euclidean distance between their beta values. Given a cluster number, ten repetitions with different random initial cluster centroids were performed in the k-means clustering algorithm to minimize the effect of the initial condition. Here, we considered cluster numbers that ranged from 2 to 10, since a cluster number greater than 10 was counterintuitive for a DMN with 32 nodes. The optimal number of clusters was determined by a winner-take-all approach across 23 effective indices using the NbClust package (Charrad et al., 2014). All of these indices were separately used to assess different aspects of the quality of the clustering.

In the main analysis, the clustering procedure was performed with the developmental rates of within-DMN degree centrality included as the features. To take into account the potential influence of other brain networks on the functional specialization of the DMN, we performed an additional k-means clustering analysis in which the clustering features were set as the developmental rates of the whole-brain degree centrality of DMN nodes. Given a node of interest, its whole-brain degree centrality was defined as the sum of the functional connectivity strength of this region with all the other gray matter voxels. A correlation threshold of 0.2 was used to discard the potential spurious connectivities (for details, see Supplementary Materials).

All network topology analyses were performed using GRETNA (www.nitrc.org/projects/gretna) (Wang et al., 2015), and the results were visualized on the brain surface using BrainNet Viewer (www.nitrc.org/projects/bnv) (Xia et al., 2013).

3. Results

3.1. Development of DMN functional connectivity in children

First, we examined the overall development of DMN functional connectivity during childhood and adolescence. Using a linear mixed model, we found that the mean connectivity strength of the DMN increased linearly with age (t = 2.35, p = 0.02, Fig. 2A). The mean connectivity strength of the DMN in children was significantly lower than that in the adults (t = −9.39, $p < 0.0001$). Furthermore, we found that the functional connectivity matrices of the DMN in children showed high spatial similarity with those of the adults (Pearson's r: 0.43 to 0.83), and the similarity increased linearly with age (t = 2.07, p = 0.04, Fig. 2A). These results suggest that both the overall connectivity strength and the spatial pattern of the DMN showed consistent developmental changes from childhood to adolescence to young adulthood.

Then, we assessed the effects of age on the functional connectivity strength for each pair of DMN nodes and observed significant linear effects. Specifically, age-related increases in connectivity strength were mainly located between the midline brain structures (e.g., between the dmPFC and PMC and between the dmPFC and vmPFC) and between PMC and MTG nodes ($q < 0.05$, FDR corrected, Fig. 2B and Table 1). Age-related decreases in connectivity were mainly located between the right anterior TPJ and bilateral hippocampus and between the left anterior TPJ and PMC (Fig. 2B and Table 2). We further explored the potential influence of internode distance on developmental changes. The intern-

Table 1
Age-related increases in functional connectivities during childhood and adolescence.

Region	Region	*t* value	*p* value	Beta value	Euclidean distance (mm)
dmPFC-1	R.vmPFC-2	5.20	2.97×10^{-7}	0.038	26.09
dmPFC-4	L.vmPFC-2	4.57	6.27×10^{-6}	0.033	26.07
dmPFC-4	PMC-3	4.17	3.59×10^{-5}	0.024	97.55
L.MTG-2	L.HC-1	4.06	5.80×10^{-5}	0.023	44.02
R.HC-1	L.MTG-2	4.00	7.19×10^{-5}	0.021	88.97
dmPFC-1	L.vmPFC-2	4.00	7.37×10^{-5}	0.029	35.95
dmPFC-1	PMC-3	3.89	1.15×10^{-4}	0.022	98.09
PMC-4	PMC-3	3.87	1.25×10^{-4}	0.019	24.93
dmPFC-4	L.vmPFC-1	3.75	1.98×10^{-4}	0.026	26.35
L.MTG-1	L.HC-1	3.75	2.00×10^{-4}	0.022	38.97
R.vmPFC-1	L.vmPFC-3	3.73	2.11×10^{-4}	0.027	27.76
dmPFC-4	R.vmPFC-1	3.73	2.16×10^{-4}	0.026	30.20
dmPFC-2	L.vmPFC-2	3.70	2.42×10^{-4}	0.031	25.82
dmPFC-2	PMC-3	3.68	2.59×10^{-4}	0.022	110.39
PMC-3	L.HC-3	3.67	2.67×10^{-4}	0.020	51.98
dmPFC-2	L.vmPFC-1	3.65	2.86×10^{-4}	0.031	20.81
dmPFC-2	R.vmPFC-2	3.61	3.35×10^{-4}	0.029	28.19
L.vmPFC-3	L.TPJ-2	3.60	3.55×10^{-4}	0.020	132.98
R.HC-1	PMC-3	3.57	3.98×10^{-4}	0.020	73.48
PMC-3	L.vmPFC-3	3.43	6.60×10^{-4}	0.019	114.10
R.HC-3	PMC-3	3.40	7.27×10^{-4}	0.018	69.12
R.vmPFC-1	R.HC-5	3.37	8.03×10^{-4}	0.016	94.45
R.HC-5	PMC-3	3.30	0.001	0.017	53.53
dmPFC-2	R.vmPFC-1	3.25	0.001	0.029	21.71
PMC-4	L.vmPFC-1	3.24	0.001	0.019	105.47
dmPFC-3	L.vmPFC-1	3.22	0.001	0.024	32.25
dmPFC-3	PMC-3	3.13	0.002	0.019	102.86
R.HC-5	L.vmPFC-2	3.13	0.002	0.014	107.00
dmPFC-1	R.vmPFC-1	3.12	0.002	0.024	25.83
R.vmPFC-3	L.vmPFC-1	3.09	0.002	0.022	27.60
PMC-3	L.HC-1	3.08	0.002	0.017	70.13
R.MTG-2	R.HC-1	3.01	0.003	0.017	41.62
L.vmPFC-2	L.HC-3	2.99	0.003	0.015	94.31
dmPFC-3	R.vmPFC-1	2.98	0.003	0.023	32.17
dmPFC-3	L.vmPFC-2	2.85	0.005	0.022	33.87
R.HC-1	L.MTG-1	2.84	0.005	0.016	86.81
R.MTG-1	PMC-3	2.84	0.005	0.015	92.25
L.MTG-2	L.HC-3	2.82	0.005	0.015	35.81

Note that all the connectivities significantly increased linearly with age, and multiple comparisons across connectivities were corrected using the FDR method with a significance level of $q < 0.05$.

Table 2
Age-related decreases in functional connectivities during childhood and adolescence.

Region	Region	*t* value	*p* value	Beta value	Euclidean distance (mm)
R.TPJ-1	R.HC-3	−4.08	5.21×10^{-5}	−0.022	50.63
R.TPJ-1	L.HC-1	−3.83	1.44×10^{-4}	−0.020	93.93
R.TPJ-1	L.HC-2	−3.75	2.00×10^{-4}	−0.020	93.50
PMC-2	L.TPJ-1	−3.72	2.23×10^{-4}	−0.025	52.00
R.TPJ-1	L.HC-3	−3.09	0.002	−0.016	88.08
R.TPJ-1	R.HC-2	−3.06	0.002	−0.016	55.62
PMC-1	L.TPJ-2	−3.05	0.002	−0.019	49.62
R.HC-4	L.TPJ-1	−3.01	0.003	−0.014	94.53
PMC-1	L.TPJ-1	−2.91	0.004	−0.020	56.64
PMC-1	L.MTG-3	−2.87	0.004	−0.017	78.92
R.HC-1	L.HC-3	−2.85	0.005	−0.014	57.79
PMC-4	L.TPJ-1	−2.82	0.005	−0.018	55.03
R.HC-5	L.HC-3	−2.81	0.005	−0.012	55.46

Note that all the connectivities significantly decreased linearly with age, and the multiple comparisons across connectivities were corrected using the FDR method with a significance level of $q < 0.05$.

ode Euclidean distances ranged from 20.81 mm to 132.98 mm (mean ± std: 59.20 ± 34.33 mm) for the age-related increased connectivities and from 49.62 mm to 94.53 mm (mean ± std: 67.83 ± 18.61 mm) for the age-related decreased connectivities (Fig. 2C). The widespread distributions of Euclidean distance in both cases indicated that the development of connectivity strength in childhood and adolescence was involved in both short- and long-range connections. Finally, we observed that most (i.e., 31/38) of the functional connectivities with significant increases from childhood to adolescence were also greater in the adults than in children ($q < 0.05$, FDR corrected, Fig. 2D) and that most (i.e., 10/13) of the connectivities with significant decreases were also lower in the adults than in the children ($q < 0.05$, FDR corrected, Fig. 2D). Simi-

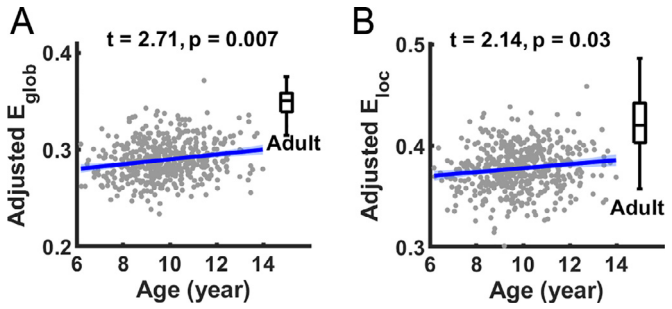

Fig. 3. Age-related increases in global efficiency (A) and local efficiency (B) of the DMN in children from 6 to 14 years old. The dots represent the adjusted values of each child after regressing out sex and head motion. The boxplots illustrate the median (horizontal line), 25th and 75th percentiles (box) and nonoutlier range (whiskers) for the adjusted values in the adult group. Both global and local efficiency were significantly higher in the adults than in the children. $E_{glob,}$ global efficiency; $E_{loc,}$ local efficiency.

lar to the aforementioned findings, these results indicated a consistent developmental trend from childhood to adolescence to adults at the connectivity level.

3.2. Increased global and local efficiency of DMN in children

We employed E_{glob} and E_{loc} measures to quantify the capability of parallel information transfer in the DMN. For children, E_{glob} of the DMN ranged from 0.22 to 0.39 and increased linearly with age (t = 2.71, p = 0.007, Fig. 3A); E_{loc} of the DMN ranged from 0.29 to 0.48 and increased linearly with age (t = 2.14, p = 0.03, Fig. 3B). Both E_{glob} and E_{loc} were significantly lower in the children than in the adults (t = 12.61, p < 0.0001 for E_{glob}; t = 11.83, p < 0.0001 for E_{loc}). These results suggest that the network integrity of the DMN was significantly elevated during development.

3.3. Development of nodal centrality in children

We calculated the degree centrality for each node to characterize the direct influence on the information communication within the DMN. Significant age-related changes in nodal degree centrality followed a linear model (q < 0.05, FDR corrected). Specifically, age-related increases were mainly located in several midline structures (e.g., the dmPFC, vmPFC, and PMC) and in the lateral region of the MTG (e.g., the left middle MTG and right posterior MTG) (q < 0.05, FDR corrected, Fig. 4A and B). All these regions showed significantly lower degree centrality in the children than in the adults (q < 0.05, FDR corrected). The spatial patterns of fitted nodal degree centrality were illustrated for children from 6 to 14 years old with a one-year interval (Fig. 4C). Highly similar spatial patterns were observed across different ages, wherein regions with high degree centrality were primarily located in the dmPFC, vmPFC, ventral PMC, and TPJ. We found that most of the regions (i.e., the dmPFC, vmPFC, and ventral/anterior PMC) with significant age-related changes also exhibited high degree centrality, regardless of the age considered. Quantitative analysis revealed a significant spatial correlation between the developmental rate of degree centrality and the average degree centrality across all children (r = 0.47, p = 0.007). All these results suggest that the development of nodal degree centrality in the DMN is primarily concentrated in the densely connected hub regions. Additionally, we also evaluated the functional roles of nodes using a metric of nodal efficiency in the aspect of parallel information communication ability. We found that nodal efficiency increased linearly with age in the dmPFC, vmPFC, PMC, MTG, and left TPJ (q < 0.05, FDR corrected, Fig. 5A and B). The nodal efficiency of these regions was significantly lower in the children than in the adults (q < 0.05, FDR corrected). Of note, the regions that showed significant age-related increases in degree centrality also exhibited significant increases in nodal efficiency (q < 0.05, FDR corrected, Fig. 5B).

3.4. Sex-related differences

With multiple comparison correction, we found that all the measurements of interest, including connectivity strength, connectivity pattern similarity, and network metrics, showed no significant sex difference or sex-by-age interaction effects (all qs > 0.05, FDR corrected).

3.5. Differentiated developmental rates of nodal centrality in DMN subclusters

We employed a k-means clustering approach to identify DMN subclusters, each of which comprised nodes with similar developmental rates of degree centrality. Fig. 6A shows the internode distance in the developmental rate of degree centrality. During the k-means clustering procedure, the optimal subcluster number was set as three, which was consistently selected by 12 of 23 effective quality indices. Fig. 6B illustrates the spatial locations of three subclusters in the DMN: cluster 1 comprised two midline structures (i.e., the vmPFC and anterior PMC); cluster 2 comprised several lateral regions (i.e., the lateral vmPFC, MTG, and posterior TPJ) and medial regions (i.e., the dmPFC and inferior PMC); cluster 3 mainly comprised the posterior PMC, hippocampus and inferior TPJ. The three clusters showed significantly different developmental rates between each other (cluster 1 vs. 2: t = 7.91, p < 0.0001; cluster 1 vs. 3: t = 12.27, p < 0.0001; cluster 2 vs. 3: t = 10.05, p < 0.0001), wherein cluster 1 showed the highest beta value, cluster 2 had the second highest beta value, and cluster 3 showed the lowest beta value (Fig. 6C). For each cluster, we separately show the developmental trajectory of one representative node, including the anterior PMC in cluster 1 (t = 4.13, p < 0.0001), the dmPFC in cluster 2 (t = 2.93, p = 0.004), and the ventral PMC in cluster 3 (t = 0.65, p = 0.52) (Fig. 6C).

To assess the potential influence of other functional networks (i.e., outside-DMN connectivity) on the clustering analysis, the developmental rates of the whole-brain degree centrality were included as the clustering features. We also detected an optimal clustering structure consisting of three subclusters (Fig. S7), which was similar to the subclusters obtained using the within-DMN degree centrality (Fig. 6) (Dice coefficient = 0.625). The most remarkable change was the spatial expansion of cluster 1: in addition to the previously identified medial regions (i.e., vmPFC and anterior PMC), the bilateral lateral vmPFC, left superior TPJ, left anterior MTG, and right posterior MTG were also included.

Next, we examined the potential differences in the developmental rate of nodal efficiency among these three clusters. Similar to the case of degree centrality, we found that these three clusters also showed significantly different developmental rates of nodal efficiency (cluster 1 vs. 2: t = 5.60, p < 0.0001; cluster 1 vs. 3: t = 8.58, p < 0.0001; cluster 2 vs. 3: t = 7.12, p < 0.0001, Fig. 7A). The developmental trajectory of one representative node is separately shown for each cluster, including the left medial vmPFC in cluster 1 (t = 3.65, p = 0.0003), the left lateral vmPFC in cluster 2 (t = 3.00, p = 0.003) and the ventral PMC in cluster 3 (t = 1.33 p = 0.19) (Fig. 7B).

3.6. Validation results

We validated our main results by generating individual functional networks with two other correlation thresholds (i.e., 0.1 and 0.3). During childhood and adolescence, the linear developmental changes in the global and nodal properties of the DMN remained nearly unchanged in these two conditions (Figs. S1–S3). The global efficiency and local efficiency significantly increased with age (all ps < 0.05, Fig. S1). The age-related increases in nodal degree centrality were primarily located at several midline structures (e.g., dmPFC, vmPFC and PMC) (q < 0.05, FDR corrected, Fig. S2A and D), which showed high degree centrality across different ages. During the clustering analysis based on the

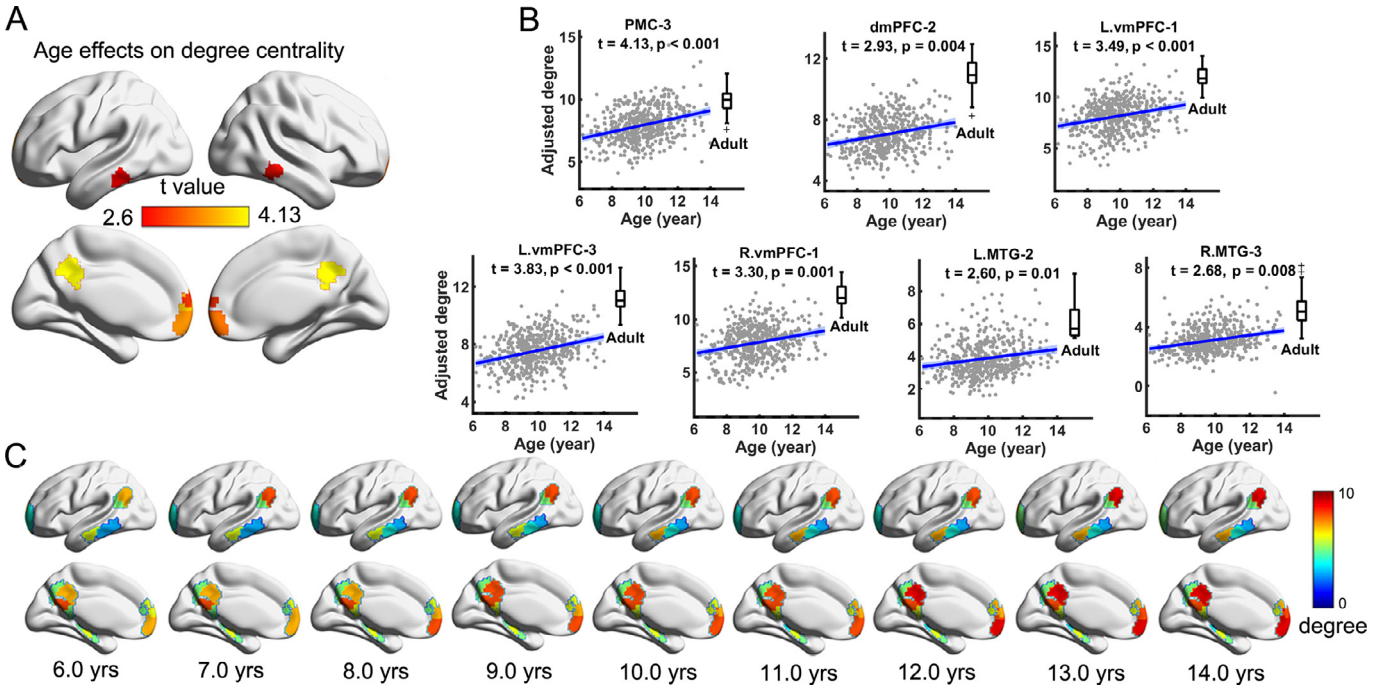

Fig. 4. Age-related changes in nodal degree in children aged 6 to 14 years old. (A) Significant effects of age on nodal degree centrality. Multiple comparisons across regions were corrected using the FDR method with a significance level of $q < 0.05$. (B) Age-related increases in degree centrality for seven regions showing significant age effects. The dots represent the adjusted values of each child after regressing out sex and head motion, and the boxplots illustrate the median (horizontal line), 25th and 75th percentiles (box) and nonoutlier range (whiskers) for the adjusted values in the adult group. (C) Fitted nodal degree for the DMN regions from ages 6 to 14 with a one-year interval. PMC-3, anterior posteromedial cingulate cortex; dmPFC-2, dorsal medial prefrontal cortex; vmPFC-1/3, medial portions of ventromedial prefrontal cortex; MTG-2/3, posterior portion of middle temporal gyrus.

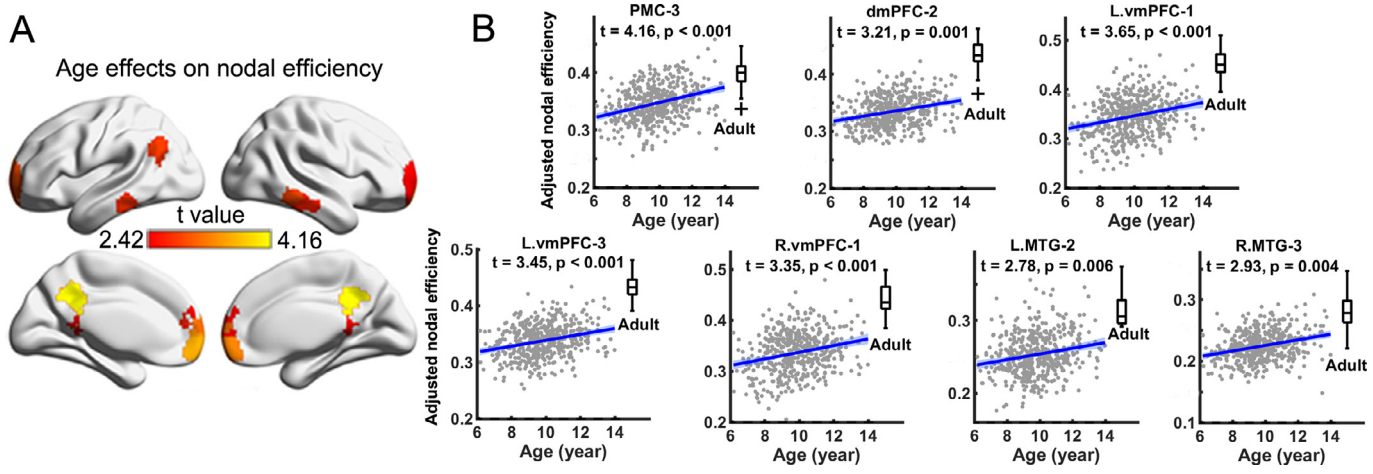

Fig. 5. Age-related changes in nodal efficiency in children aged 6 to 14 years old. (A) Significant effects of age on nodal efficiency. Multiple comparisons were corrected using the FDR method with a significance level of $q < 0.05$. (B) Age-related increases in nodal efficiency for seven regions that showed significant age effects on nodal degree. The dots represent the adjusted values of each child after regressing out sex and head motion, and the boxplots illustrate the median (horizontal line), 25th and 75th percentiles (box) and nonoutlier range (whiskers) for the adjusted values in the adult group. PMC-3, anterior posteromedial cingulate cortex; dmPFC-2, dorsal medial prefrontal cortex; vmPFC-1/3, medial portions of ventromedial prefrontal cortex; MTG-2/3, posterior portion of middle temporal gyrus.

regional developmental rates of nodal degree centrality, we identified three subclusters showing differentiated developmental rates within the DMN at correlation thresholds of 0.1 and 0.3 (Fig. S3B and E), which agreed well with those in the main results (Fig. 6B).

4. Discussion

In this study, we used a large longitudinal rsfMRI sample to examine the development of the intrinsic functional organization of the DMN from childhood to adolescence. We found a linear maturational trajectory in the DMN toward the adult-like architecture from childhood to adolescence. Specifically, these changes were mainly localized between regions at the midline structures. The network efficiency of the DMN also increased from childhood to adolescence. We identified three DMN subclusters based on divergent developmental rate of degree centrality, with the fastest development in one cluster mainly comprising two regions (e.g., the anterior mPFC and PCC) in the midline structures. Together, our findings suggest the enhancement of functional integration

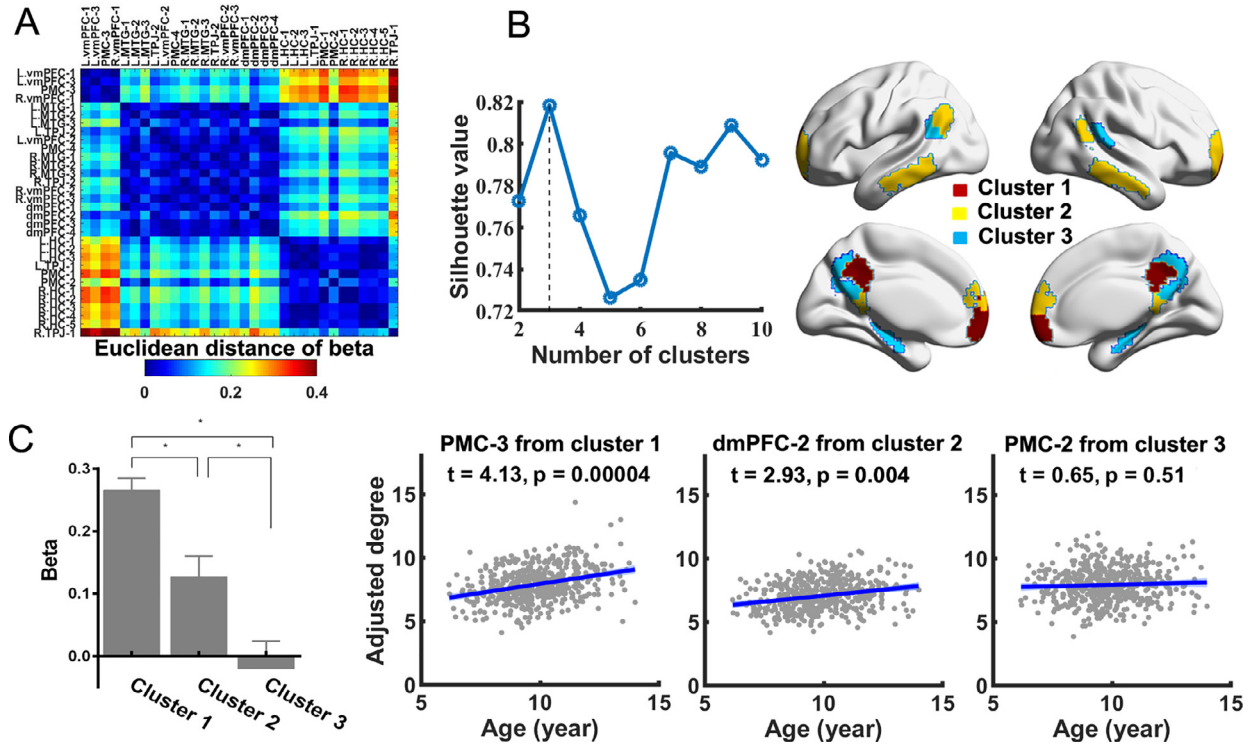

Fig. 6. Subcluster classification of the DMN in children. (A) Interregional differences in the developmental rate of degree centrality in terms of the Euclidean distance between beta values of the age effects. (B) Dependence of the silhouette value on the selection of cluster number and the spatial locations of the three subclusters. The optimal subcluster number (i.e., three) was consistently selected by 12 of 23 effective quality indices. (C) Differences in the developmental rate of degree centrality among the three clusters. Significant differences were observed between each pair of clusters (all $qs < 0.05$, FDR corrected). For each cluster, the age-related change for one node is displayed. The dots represent the adjusted values of each child after regressing out sex and head motion. PMC-3, anterior posteromedial cingulate cortex; dmPFC-2, dorsal medial prefrontal cortex; PMC-2, ventral posteromedial cingulate cortex.

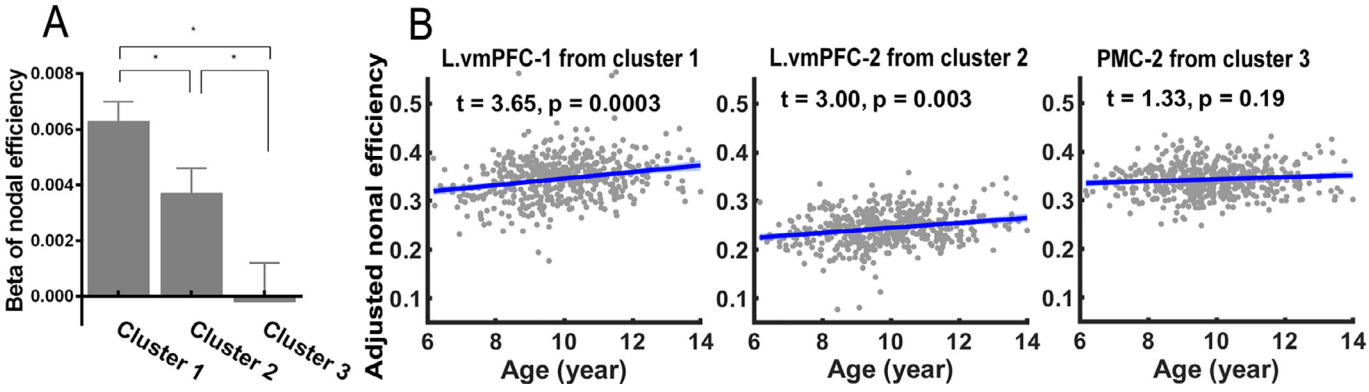

Fig. 7. Divergent developmental rates of nodal efficiency for the three identified subclusters. (A) Differences in the developmental rate of nodal efficiency among the three clusters. Significant differences were observed between each pair of clusters (all $qs < 0.05$, FDR corrected). (B) For each cluster, the age-related change for one region is displayed. The dots represent the adjusted values of each child after regressing out sex and head motion. L.vmPFC-1, left medial portion of the ventromedial prefrontal cortex; L.vmPFC-2, left lateral portion of the ventromedial prefrontal cortex; PMC-2, ventral posteromedial cingulate cortex.

and efficiency in the DMN from childhood to adolescence and into adulthood accompanied by regional inhomogeneity in developmental rates.

4.1. Functional connectivity and network efficiency of the DMN changed with age

Based on the cross-sectional design, several previous studies have revealed age-related increases in the functional connectivity strength of the DMN during the school-age period of development (de Bie et al., 2012; Mak et al., 2017; Sato et al., 2014; Sherman et al., 2014) and between 7 to 9-year-old children and adults (Fair et al., 2008). Of note, the developmental changes observed in these studies could be contaminated by intersubject variability. Using task-related (i.e., passive listening) fMRI data of a small sample ($N = 45$), a recent longitudinal study reported an age-related increase in the functional connectivity strength of the PCC within the DMN for children from 10 to 13 years old (Sherman et al., 2014). In the current study, to reduce the influence of intersubject variability and to increase statistical power, we employed a large sample of longitudinal rsfMRI data and revealed continuous age effects of age on the intrinsic functional organization of the DMN. We found that the overall connectivity strength of the DMN linearly increased with age during childhood and adolescence, wherein the age-related increased connectivities were mainly localized between midline structures (e.g., between the mPFC and PMC) (Fig. 2B). Consistent

findings have also been observed in previous rsfMRI studies (Fair et al., 2008; Sato et al., 2014; Sherman et al., 2014). In addition, we found that the global and local network efficiency of the DMN increased with age (Fig. 3). All these findings suggest that the functional integration of the DMN was elevated during childhood and adolescence, accompanied by an increased capability regarding parallel information transfer and fault tolerance. Accumulating evidence in adults suggests that DMN functional connectivity strength is positively correlated with multiple cognitive functions, such as working memory (Hampson et al., 2006; Liu et al., 2017; Prakash et al., 2012; Sambataro et al., 2010), autobiographical memory (Mevel et al., 2013), mental manipulation (Yang et al., 2013), and language (Yang et al., 2013). We speculate that the age-related increases in functional integrative capacity within the DMN observed here could facilitate individual cognition improvements in children, which needs to be further explored by including cognitive and behavioral measures.

The age-related increases in functional connectivity of midline structures may be shaped by the underlying anatomical structures. Using multimodal MRI data, several previous studies have identified some structural fiber pathways within the DMN in both children and adults, such as PCC projections to the mPFC and bilateral MTL (Greicius et al., 2009). Both functional connectivity strength and fiber density between the PCC and mPFC were lower in children (7 to 9 years) than in adults (Supekar et al., 2010), indicating a consistent developmental trend in functional and structural connectivity from childhood to adulthood. Diffusion MRI studies also revealed that the structural connectivity strength of the cingulum bundle between the PCC and mPFC increased with age (Clayden et al., 2012; Imperati et al., 2011; Tamnes et al., 2010). Thus, structural connectivity development within the DMN is likely to underlie functional connectivity development in this system.

Different from the existing studies, in addition to the age-related increases, we also observed age-related decreases in functional connectivity strength (Fig. 2B). These strength decreases were mainly located between the right anterior TPJ and bilateral hippocampus and between the left anterior TPJ and PMC, suggesting increased functional segregation between the TPJ and the other regions. Previous studies have reported that the TPJ, hippocampus, and PMC are engaged in different functions, including theory of mind, autobiographical memory and self-referential thinking (Andrews-Hanna et al., 2014; DuPre et al., 2016). The age-related decreases reflected the increasing functional specialization of these brain regions during development.

4.2. Subclusters of the DMN with divergent developmental rates in degree centrality

The adult DMN can be divided into two or three separate subnetworks (e.g., the core subsystem, dmPFC subsystem, and MTL subsystem) with functionally specialized roles (Andrews-Hanna et al., 2010; Braga and Buckner, 2017; Braga et al., 2019; Buckner and DiNicola, 2019). This reflects functional segregation within the DMN. Here, we observed spatial heterogeneity in the developmental trajectories of degree centrality of the DMN regions. Most of the regions (i.e., the dmPFC, vmPFC, and PMC) with significant effects of age were located in the midline structures (Fig. 4A), which is consistent with the observation at the connectivity level (Fig. 2B). These regions consistently exhibited high degree centrality across different ages, suggesting that the regions playing crucial roles in information integration undergo rapid development. Furthermore, we found that the DMN is differentiated into three subclusters (Fig. 6B) based on spatial heterogeneity in the developmental rate of nodal degree centrality, which was spatially similar to the three subnetworks in adults (Andrews-Hanna et al., 2010; Buckner and DiNicola, 2019) Specifically, in this study, cluster 1 was similar to the core subsystem in adults, cluster 2 was similar to the dmPFC subsystem, and cluster 3 was similar to the MTL subsystem (Andrews-Hanna et al., 2010). The spatial heterogeneity in the developmental rates and the presence of subclusters were consistently observed at different correlation thresholds (i.e., r_{th} = 0.1, 0.2 and 0.3) (Figs. 4, 6, S2 and S3), while a high correlation threshold tended to reveal a more fine-grained subdivision of the DMN. Our findings indicate that different subsystems have differentiated developmental trajectories, which represent the functional specialization within the DMN. Of note, these subclusters were identified based on the divergent developmental rates of nodal degree centrality within the DMN. When considering the developmental rates of whole-brain degree centrality, we found that the clustering structure was generally similar to that observed within the DMN (Fig. S7). However, there were slight differences between the two analyses, which were predominantly located in the bilateral lateral vmPFC, left superior TPJ, left anterior MTG, and right posterior MTG.

Such a specialization of the DMN could be related to the divergent anatomical connectivity among regions. This was supported by previous studies, which demonstrated that the spatial gradient in the strength of parahippocampal projections biases the protoorganization of DMN regions to fractionate into distinct, specialized networks (Buckner and DiNicola, 2019). In this study, we also observed that there was regional heterogeneity in the structural developmental characteristics within the DMN and that this structural development was different from the functional development of the DMN (Fig. S4). Specifically, we found that cluster 2 showed a significantly lower age at peak and a larger developmental rate in the gray matter volume than cluster 3 (Fig. S5). This suggests that earlier structural maturation and faster structural changes in gray matter volume might promote faster functional development (Fig. S6).

Children rapidly develop internal cognitive processes, including autobiographical memory (Given-Wilson et al., 2018) and theory of mind (Devine and Hughes, 2013; Dumontheil et al., 2010; O'Connor and Evans, 2019). These different processes are involved in different brain regions. Functional imaging studies in adults showed that autobiographical memory tasks preferentially involved the parahippocampal cortex and the ventral portion of the posterior midline (DuPre et al., 2016; Spreng and Grady, 2010), which spatially overlapped with the cluster 3 obtained in our study. Nevertheless, theory of mind-related tasks preferentially involve anterior region of the TPJ (Andrews-Hanna et al., 2014; DuPre et al., 2016; Spreng and Grady, 2010). We propose that the developmental rate of subnetworks is accompanied by the development of self-related and social-cognitive functions that improve during childhood and adolescence; nonetheless, this relationship warrants further investigation.

Sex plays a critical role in the development of the topological organization of functional networks (Gong et al., 2009; Wu et al., 2013). Here, we examined potential sex effects on DMN topology and its development in children. No significant sex effect was observed for all measurements of interest, suggesting that boys and girls exhibited similar DMN properties and developmental changes from childhood to adolescence. Similar to our study, no significant sex effect was observed in DMN functional connectivity in adults (Weissman-Fogel et al., 2010). Notably, one study reported significant sex-related differences in the nodal degree of the default mode network in 6-20 years old (Wu et al., 2013). The inconsistency between this study and our findings might be due to the different age ranges considered or different strategies for estimating the nodal properties.

4.3. Further considerations

Several issues need to be further considered. First, we defined nodes of interest of the DMN according to a prior atlas of the DMN in adults that delineates regional-level gray-matter subdivisions within the DMN (Kernbach et al., 2018), implicitly assuming the same spatial locations of DMN nodes across the whole population of children. However, the spatial distributions of the DMN may change during development (Cui et al., 2020) and vary across individuals even at the same age (Laumann et al., 2015; Liao et al., 2017). The temporal evolution and intersubject variability in the spatial distribution should be taken into account in future

studies to better capture DMN development. Second, previous studies have shown that head motion can bias the estimation of interregional functional connectivity (Power et al., 2012) and thus affect developmental findings (Satterthwaite et al., 2012). To reduce the influence of head motion, we included 24 head motion parameters (Friston et al., 1996), the global brain signal (Satterthwaite et al., 2012; Yan et al., 2013), and scrubbing-based spiking (Satterthwaite et al., 2013) in the nuisance regression of the data preprocessing. In addition, the mean FD parameter (Power et al., 2012) was also included as a covariate in the linear mixed model when assessing the age effects. However, the residual effect of head motion may still exist, and this issue requires the development of advanced strategies for head motion correction. Third, in this study, we focused on the developmental characteristics of the connectivity patterns within the DMN. In addition to the DMN, other functional networks also undergo remarkable changes from childhood to adolescence, which could be related to the development of the DMN. For instance, during childhood and adolescence, the connectivity strength in the DMN and central executive network increases with age (Sato et al., 2014; Sherman et al., 2014), while the anticorrelation between these two networks is strengthened with age (Sherman et al., 2014). Considering the potential influence of the outside-DMN connectivities on DMN specialization (Fig. S7), the detailed relationships between the development of the DMN subclusters and the other networks need to be explored in the future. Fourth, we used rsfMRI to explore the development of the intrinsic functional organization of the DMN. Previous studies have demonstrated the structural correlates of the functional coupling of the DMN in adults (Greicius et al., 2009; Kernbach et al., 2018). However, this relationship during the developmental stage of childhood and adolescence remains elusive. Here, we performed a structural MRI analysis to explore the potential influence of regional heterogeneity in gray matter volume development on the functional specialization of the DMN. In future studies, the fusion of multimodal data is recommended to comprehensively study the structural basis of the functional development of the DMN. Fifth, studies in adults have demonstrated that the connectivity strength of the DMN is positively correlated with several cognitive functions (Hampson et al., 2006; Mevel et al., 2013; Persson et al., 2014; Prakash et al., 2012; Sambataro et al., 2010; Yang et al., 2013), leading to the speculation that the strengthened functional integration of the DMN during childhood and adolescence is related to individual cognitive improvements. It would be worthwhile to explore the relationship between cognitive improvement and DMN development in the future.

Declaration of Competing Interest

The authors have declared that no conflicting interests exist.

Acknowledgments

The study was supported by the National Natural Science Foundation of China (Nos. 31830034, 81971690, 81620108016, 11835003, 31221003, 31521063, and 82021004), Changjiang Scholar Professorship Award (T2015027), the Beijing Brain Initiative of Beijing Municipal Science & Technology Commission (Z181100001518003), and the Fundamental Research Funds for the Central Universities (2019NTST24). We thank the National Center for Protein Sciences at Peking University in Beijing, China, for assistance with MRI data acquisition.

Data and code availability statement

In this study, the authors used a longitudinal resting-state functional MRI data from the Children School Functions and Brain Development project (CBD, Beijing Cohort). Some study data and codes are available at GitHub (https://github.com/fanfengmei/CBD-BNU-DMN).

Credit author statement

Fengmei Fan, Xuhong Liao, Shaozheng Qin, Sha Tao, Qi Dong, and Yong He conceived and designed the study; Weiwei Men, Yanpei Wang, Mingming Hu, Jie Liu, Shuping Tan, Jia-Hong Gao, and Sha Tao collected the data; Fengmei Fan, Xuhong Liao, and Tianyuan Lei performed the data analysis with technical support from Tengda Zhao and Mingrui Xia; Fengmei Fan, Xuhong Liao, and Yong He wrote the manuscript; all authors commented on the study and manuscript.

Supplementary materials

Supplementary material associated with this article can be found, in the online version, at doi:10.1016/j.neuroimage.2020.117581.

References

Achard, S., Bullmore, E., 2007. Efficiency and cost of economical brain functional networks. PLoS Comput. Biol. 3, e17.
Akaike, H., 1974. A new look at the statistical model identification. IEEE Trans. Autom. Control 19, 8.
Andrews-Hanna, J.R., Reidler, J.S., Sepulcre, J., Poulin, R., Buckner, R.L., 2010. Functional-anatomic fractionation of the brain's default network. Neuron 65, 550–562.
Andrews-Hanna, J.R., Saxe, R., Yarkoni, T., 2014. Contributions of episodic retrieval and mentalizing to autobiographical thought: evidence from functional neuroimaging, resting-state connectivity, and fMRI meta-analyses. NeuroImage 91, 324–335.
Bernal-Rusiel, J.L., Greve, D.N., Reuter, M., Fischl, B., Sabuncu, M.R., Neuroimaging, Alzheimer's Disease, 2013. Statistical analysis of longitudinal neuroimage data with linear mixed effects models. NeuroImage 66, 249–260.
Bhana, A., 2010. Middle Chilldhood and Pre-Adolescence. HSRC Press.
Blakemore, S.J., 2008. The social brain in adolescence. Nat. Rev.: Neurosci. 9, 267–277.
Blakemore, S.J., Burnett, S., Dahl, R.E., 2010. The role of puberty in the developing adolescent brain. Hum. Brain Mapp. 31, 926–933.
Braga, R.M., Buckner, R.L., 2017. Parallel interdigitated distributed networks within the individual estimated by intrinsic functional connectivity. Neuron 95, 457–471 e455.
Braga, R.M., Van Dijk, K.R.A., Polimeni, J.R., Eldaief, M.C., Buckner, R.L., 2019. Parallel distributed networks resolved at high resolution reveal close juxtaposition of distinct regions. J. Neurophysiol. 121, 1513–1534.
Buckner, R.L., Andrews-Hanna, J.R., Schacter, D.L., 2008. The brain's default network: anatomy, function, and relevance to disease. Ann. N. Y. Acad. Sci. 1124, 1–38.
Buckner, R.L., DiNicola, L.M., 2019. The brain's default network: updated anatomy, physiology and evolving insights. Nat. Rev.: Neurosci. 20, 593–608.
Buckner, R.L., Sepulcre, J., Talukdar, T., Krienen, F.M., Liu, H., Hedden, T., Andrews-Hanna, J.R., Sperling, R.A., Johnson, K.A., 2009. Cortical hubs revealed by intrinsic functional connectivity: mapping, assessment of stability, and relation to Alzheimer's disease. J. Neurosci. 29, 1860–1873.
Casey, B.J., Giedd, J.N., Thomas, K.M., 2000. Structural and functional brain development and its relation to cognitive development. Biol. Psychol. 54, 241–257.
Charrad, M., Ghazzali, N., Boiteau, V., Niknafs, A., 2014. NbClust: an R package for determining the relevant number of clusters in a data set. J. Stat. Softw. 61, 36.
Clayden, J.D., Jentschke, S., Munoz, M., Cooper, J.M., Chadwick, M.J., Banks, T., Clark, C.A., Vargha-Khadem, F., 2012. Normative development of white matter tracts: similarities and differences in relation to age, gender, and intelligence. Cereb. Cortex 22, 1738–1747.
Cui, Z., Li, H., Xia, C.H., Larsen, B., Adebimpe, A., Baum, G.L., Cieslak, M., Gur, R.E., Gur, R.C., Moore, T.M., Oathes, D.J., Alexander-Bloch, A.F., Raznahan, A., Roalf, D.R., Shinohara, R.T., Wolf, D.H., Davatzikos, C., Bassett, D.S., Fair, D.A., Fan, Y., Satterthwaite, T.D., 2020. Individual variation in functional topography of association networks in youth. Neuron 106, 340–353 e348.
Cushman, F., Sheketoff, R., Wharton, S., Carey, S., 2013. The development of intent-based moral judgment. Cognition 127, 6–21.
de Bie, H.M., Boersma, M., Adriaanse, S., Veltman, D.J., Wink, A.M., Roosendaal, S.D., Barkhof, F., Stam, C.J., Oostrom, K.J., Delemarre-van de Waal, H.A., Sanz-Arigita, E.J., 2012. Resting-state networks in awake five- to eight-year old children. Hum. Brain Mapp. 33, 1189–1201.
Devine, R.T., Hughes, C., 2013. Silent films and strange stories: theory of mind, gender, and social experiences in middle childhood. Child Dev. 84, 989–1003.
Dong, Q., Lin, C., 2011. Standardized Tests of the National Children's Study of China. Science Press, Beijing.
Dumontheil, I., Apperly, I.A., Blakemore, S.J., 2010. Online usage of theory of mind continues to develop in late adolescence. Dev. Sci. 13, 331–338.
DuPre, E., Luh, W.M., Spreng, R.N., 2016. Multi-echo fMRI replication sample of autobiographical memory, prospection and theory of mind reasoning tasks. Sci. Data 3, 160116.
Fair, D.A., Cohen, A.L., Dosenbach, N.U., Church, J.A., Miezin, F.M., Barch, D.M., Raichle, M.E., Petersen, S.E., Schlaggar, B.L., 2008. The maturing architecture of the brain's default network. In: Proceedings of the National Academy of Sciences of the United States of America, 105, pp. 4028–4032.
Fair, D.A., Cohen, A.L., Power, J.D., Dosenbach, N.U., Church, J.A., Miezin, F.M., Schlaggar, B.L., Petersen, S.E., 2009. Functional brain networks develop from a "local to distributed" organization. PLoS Comput. Biol. 5, e1000381.

Fox, M.D., Snyder, A.Z., Vincent, J.L., Corbetta, M., Van Essen, D.C., Raichle, M.E., 2005. The human brain is intrinsically organized into dynamic, anticorrelated functional networks. In: Proceedings of the National Academy of Sciences of the United States of America, 102, pp. 9673–9678.
Friston, K.J., Williams, S., Howard, R., Frackowiak, R.S., Turner, R., 1996. Movement-related effects in fMRI time-series. Magn. Reson. Med. 35, 346–355.
Gaspar, P.M., Bautch, J.C., Strodthoff, C.M., 2015. A longitudinal study of the health status of a community of religious sisters: addressing the advantages, challenges, and limitations. Res. Gerontol. Nurs. 8, 77–84.
Gilbert, D.T., Wilson, T.D., 2007. Prospection: experiencing the future. Science 317, 1351–1354.
Given-Wilson, Z., Hodes, M., Herlihy, J., 2018. A review of adolescent autobiographical memory and the implications for assessment of unaccompanied minors' refugee determinations. Clin. Child Psychol. Psychiatry 23, 209–222.
Gong, G., He, Y., Concha, L., Lebel, C., Gross, D.W., Evans, A.C., Beaulieu, C., 2009. Mapping anatomical connectivity patterns of human cerebral cortex using in vivo diffusion tensor imaging tractography. Cereb. Cortex 19, 524–536.
Greicius, M.D., Krasnow, B., Reiss, A.L., Menon, V., 2003. Functional connectivity in the resting brain: a network analysis of the default mode hypothesis. In: Proceedings of the National Academy of Sciences of the United States of America, 100, pp. 253–258.
Greicius, M.D., Supekar, K., Menon, V., Dougherty, R.F., 2009. Resting-state functional connectivity reflects structural connectivity in the default mode network. Cereb. Cortex 19, 72–78.
Gusnard, D.A., Akbudak, E., Shulman, G.L., Raichle, M.E., 2001. Medial prefrontal cortex and self-referential mental activity: relation to a default mode of brain function. In: Proceedings of the National Academy of Sciences of the United States of America, 98, pp. 4259–4264.
Hampson, M., Driesen, N.R., Skudlarski, P., Gore, J.C., Constable, R.T., 2006. Brain connectivity related to working memory performance. J. Neurosci. 26, 13338–13343.
Hwang, K., Hallquist, M.N., Luna, B., 2013. The development of hub architecture in the human functional brain network. Cereb. Cortex 23, 2380–2393.
Imperati, D., Colcombe, S., Kelly, C., Martino, Di, A., Zhou, J., Castellanos, F.X., Milham, 2011. Differential development of human brain white matter tracts. PloS One 6, e23437.
Kernbach, J.M., Yeo, B.T.T., Smallwood, J., Margulies, D.S., Thiebaut de Schotten, M., Walter, H., Sabuncu, M.R., Holmes, A.J., Gramfort, A., Varoquaux, G., Thirion, B., Bzdok, D., 2018. Subspecialization within default mode nodes characterized in 10,000 UK Biobank participants. In: Proceedings of the National Academy of Sciences of the United States of America, 115, pp. 12295–12300.
Kutluturk Karagoz, I., Keskin, B., Ozkalayci, F., Karagoz, A., 2019. Linear mixed model better than repeated measures analysis. Eur. J. Ophthalmol. 1120672119890518.
Laird, N.M., Ware, J.H., 1982. Random-effects models for longitudinal data. Biometrics 38, 963–974.
Latora, V., Marchiori, M., 2001. Efficient behavior of small-world networks. Phys. Rev. Lett. 87, 198701.
Laumann, T.O., Gordon, E.M., Adeyemo, B., Snyder, A.Z., Joo, S.J., Chen, M.Y., Gilmore, A.W., McDermott, K.B., Nelson, S.M., Dosenbach, N.U., Schlaggar, B.L., Mumford, J.A., Poldrack, R.A., Petersen, S.E., 2015. Functional system and areal organization of a highly sampled individual human brain. Neuron 87, 657–670.
Liang, X., Zou, Q., He, Y., Yang, Y., 2013. Coupling of functional connectivity and regional cerebral blood flow reveals a physiological basis for network hubs of the human brain. In: Proceedings of the National Academy of Sciences of the United States of America, 110, pp. 1929–1934.
Liao, X., Cao, M., Xia, M., He, Y., 2017. Individual differences and time-varying features of modular brain architecture. NeuroImage 152, 94–107.
Liao, X.H., Xia, M.R., Xu, T., Dai, Z.J., Cao, X.Y., Niu, H.J., Zuo, X.N., Zang, Y.F., He, Y., 2013. Functional brain hubs and their test-retest reliability: a multiband resting-state functional MRI study. NeuroImage 83, 969–982.
Liu, J., Xia, M., Dai, Z., Wang, X., Liao, X., Bi, Y., He, Y., 2017. Intrinsic brain hub connectivity underlies individual differences in spatial working memory. Cereb. Cortex 27, 5496–5508.
Mak, L.E., Minuzzi, L., MacQueen, G., Hall, G., Kennedy, S.H., Milev, R., 2017. The default mode network in healthy individuals: a systematic review and meta-analysis. Brain Connect. 7, 25–33.
Mevel, K., Landeau, B., Fouquet, M., Joie, R.L., Villain, N., Mezenge, F., Perrotin, A., Eustache, F., Desgranges, B., Chetelat, G., 2013. Age effect on the default mode network, inner thoughts, and cognitive abilities. Neurobiol. Aging 34, 1292–1301.
Nelson, E.E., Leibenluft, E., McClure, E.B., Pine, D.S., 2005. The social re-orientation of adolescence: a neuroscience perspective on the process and its relation to psychopathology. Psychol. Med. 35, 163–174.
Newman, A.B., 2010. An overview of the design, implementation, and analyses of longitudinal studies on aging. J. Am. Geriatr. Soc. 58 Suppl 2, S287-291.
O'Connor, A.M., Evans, A.D., 2019. The role of theory of mind and social skills in predicting children's cheating. J. Exp. Child Psychol. 179, 337–347.
Onnela, J.P., Saramaki, J., Kertesz, J., Kaski, K., 2005. Intensity and coherence of motifs in weighted complex networks. Phys. Rev. E: Stat. Nonlinear Soft Matter Phys. 71, 065103.
Persson, J., Pudas, S., Nilsson, L.G., Nyberg, L., 2014. Longitudinal assessment of default-mode brain function in aging. Neurobiol. Aging 35, 2107–2117.
Power, J.D., Barnes, K.A., Snyder, A.Z., Schlaggar, B.L., Petersen, S.E., 2012. Spurious but systematic correlations in functional connectivity MRI networks arise from subject motion. NeuroImage 59, 2142–2154.
Prakash, R.S., Heo, S., Voss, M.W., Patterson, B., Kramer, A.F., 2012. Age-related differences in cortical recruitment and suppression: implications for cognitive performance. Behav. Brain Res. 230, 192–200.
Raichle, M.E., 2015. The brain's default mode network. Annu. Rev. Neurosci. 38, 433–447.
Raichle, M.E., MacLeod, A.M., Snyder, A.Z., Powers, W.J., Gusnard, D.A., Shulman, G.L., 2001. A default mode of brain function. In: Proceedings of the National Academy of Sciences of the United States of America, 98, pp. 676–682.
Rebello, K., Moura, L.M., Pinaya, W.H.L., Rohde, L.A., Sato, J.R., 2018. Default mode network maturation and environmental adversities during childhood. Chron. Stress 2, 2470547018808295.
Rochat, P., 2011. The self as phenotype. Conscious. Cognit. 20, 109–119.
Sambataro, F., Murty, V.P., Callicott, J.H., Tan, H.Y., Das, S., Weinberger, D.R., Mattay, V.S., 2010. Age-related alterations in default mode network: impact on working memory performance. Neurobiol. Aging 31, 839–852.
Sato, J.R., Salum, G.A., Gadelha, A., Picon, F.A., Pan, P.M., Vieira, G., Zugman, A., Hoexter, M.Q., Anes, M., Moura, L.M., Del'Aquilla, M.A.G., Amaro Jr., E., McGuire, P., Crossley, N., Lacerda, A., Rohde, L.A., Miguel, E.C., Bressan, R.A., Jackowski, A.P., 2014. Age effects on the default mode and control networks in typically developing children. J. Psychiatr. Res. 58, 89–95.
Sato, S.M., Schulz, K.M., Sisk, C.L., Wood, R.I., 2008. Adolescents and androgens, receptors and rewards. Horm. Behav. 53, 647–658.
Satterthwaite, T.D., Elliott, M.A., Gerraty, R.T., Ruparel, K., Loughead, J., Calkins, M.E., Eickhoff, S.B., Hakonarson, H., Gur, R.C., Gur, R.E., Wolf, D.H., 2013. An improved framework for confound regression and filtering for control of motion artifact in the preprocessing of resting-state functional connectivity data. NeuroImage 64, 240–256.
Satterthwaite, T.D., Wolf, D.H., Loughead, J., Ruparel, K., Elliott, M.A., Hakonarson, H., Gur, R.C., Gur, R.E., 2012. Impact of in-scanner head motion on multiple measures of functional connectivity: relevance for studies of neurodevelopment in youth. NeuroImage 60, 623–632.
Seber, G.A., 2009. Multivariate Observations. John Wiley & Sons.
Sherman, L.E., Rudie, J.D., Pfeifer, J.H., Masten, C.L., McNealy, K., Dapretto, M., 2014. Development of the default mode and central executive networks across early adolescence: a longitudinal study. Dev. Cognit. Neurosci. 10, 148–159.
Shulman, G.L., Fiez, J.A., Corbetta, M., Buckner, R.L., Miezin, F.M., Raichle, M.E., Petersen, S.E., 1997. Common blood flow changes across visual tasks: II. Decreases in cerebral cortex. J. Cognit. Neurosci. 9, 648–663.
Spreng, R.N., Grady, C.L., 2010. Patterns of brain activity supporting autobiographical memory, prospection, and theory of mind, and their relationship to the default mode network. J. Cognit. Neurosci. 22, 1112–1123.
Spreng, R.N., Mar, R.A., Kim, A.S., 2009. The common neural basis of autobiographical memory, prospection, navigation, theory of mind, and the default mode: a quantitative meta-analysis. J. Cognit. Neurosci. 21, 489–510.
Supekar, K., Uddin, L.Q., Prater, K., Amin, H., Greicius, M.D., Menon, V., 2010. Development of functional and structural connectivity within the default mode network in young children. NeuroImage 52, 290–301.
Tamnes, C.K., Ostby, Y., Fjell, A.M., Westlye, L.T., Due-Tonnessen, P., Walhovd, K.B., 2010. Brain maturation in adolescence and young adulthood: regional age-related changes in cortical thickness and white matter volume and microstructure. Cereb. Cortex 20, 534–548.
van den Heuvel, M.P., Sporns, O., 2013. Network hubs in the human brain. Trends Cognit. Sci. 17, 683–696.
Wang, J., Wang, X., Xia, M., Liao, X., Evans, A., He, Y., 2015. GRETNA: a graph theoretical network analysis toolbox for imaging connectomics. Front. Hum. Neurosci. 9, 386.
Weissman-Fogel, I., Moayedi, M., Taylor, K.S., Pope, G., Davis, K.D., 2010. Cognitive and default-mode resting state networks: do male and female brains "rest" differently? Hum. Brain Mapp. 31, 1713–1726.
Wig, G.S., Schlaggar, B.L., Petersen, S.E., 2011. Concepts and principles in the analysis of brain networks. Ann. N. Y. Acad. Sci. 1224, 126–146.
Wu, K., Taki, Y., Sato, K., Hashizume, H., Sassa, Y., Takeuchi, H., Thyreau, B., He, Y., Evans, A.C., Li, X., Kawashima, R., Fukuda, H., 2013. Topological organization of functional brain networks in healthy children: differences in relation to age, sex, and intelligence. PloS One 8, e55347.
Xia, M., Wang, J., He, Y., 2013. BrainNet Viewer: a network visualization tool for human brain connectomics. PloS One 8, e68910.
Xiao, Y., Zhai, H., Friederici, A.D., Jia, F., 2016. The development of the intrinsic functional connectivity of default network subsystems from age 3 to 5. Brain Imaging Behav. 10, 50–59.
Yan, C.G., Cheung, B., Kelly, C., Colcombe, S., Craddock, R.C., Martino, Di, A., Li, Q., Zuo, X.N., Castellanos, F.X., Milham, 2013. A comprehensive assessment of regional variation in the impact of head micromovements on functional connectomics. NeuroImage 76, 183–201.
Yan, C.G., Wang, X.D., Zuo, X.N., Zang, Y.F., 2016. DPABI: data processing & analysis for (resting-state) brain imaging. NeuroInformatics 14, 339–351.
Yang, A.C., Huang, C.C., Yeh, H.L., Liu, M.E., Hong, C.J., Tu, P.C., Chen, J.F., Huang, N.E., Peng, C.K., Lin, C.P., Tsai, S.J., 2013. Complexity of spontaneous BOLD activity in default mode network is correlated with cognitive function in normal male elderly: a multiscale entropy analysis. Neurobiol. Aging 34, 428–438.
Zhao, T., Liao, X., Fonov, V.S., Wang, Q., Men, W., Wang, Y., Qin, S., Tan, S., Gao, J.H., Evans, A., Tao, S., Dong, Q., He, Y., 2019. Unbiased age-specific structural brain atlases for Chinese pediatric population. NeuroImage 189, 55–70.